Solar Energy Materials & Solar Cells 238 (2022) 111611

Contents lists available at ScienceDirect

Solar Energy Materials and Solar Cells

journal homepage: www.elsevier.com/locate/solmat

An integrated multifunctional membrane via broadband light modulation for greenhouse smart windows

Yang Liu [a,b], Shaoxin Song [a], Hyunsik Yoon [c], Mingxia Liu [a], Lili Yang [a,*], Dengteng Ge [b]

[a] State Key Laboratory for Modification of Chemical Fibers and Polymer Materials, College of Materials Science and Engineering, Donghua University, Shanghai, 201620, China
[b] State Key Laboratory for Modification of Chemical Fibers and Polymer Materials, Institute of Functional Materials, Donghua University, Shanghai, 201620, China
[c] Department of Chemical and Biomolecular Engineering, Seoul National University of Science & Technology, Seoul, 01811, South Korea

ARTICLE INFO

Keywords:
Broadband light modulation
Smart windows
UV blocking
IR shielding
Visible tuning
Greenhouse

ABSTRACT

Smart windows that regulate solar irradiation (including ultraviolet UV, visible and infrared) have emerged as an exciting research area for energy conservation, privacy protection and organism healthcare. However, scalable, low cost and robust smart windows with broadband light modulation are still challengeable for practical applications. Here, an integrated smart membrane with capability of managing the light wavelength from UV, visible (Vis) to near infrared (NIR) band via facile spray coating is reported. The smart membrane consists of the upper ITO rich layer, bottom TiO_2/SiO_2 NPs layer and a bulk elastomeric PDMS as matrix. Due to the NIR reflection and UV absorption, the smart membrane shows high Vis transmittance and moderate UV and NIR transmittance under relaxed state. Due to Mie scattering from vacuum cavity, under stretching (50%), UV, Vis and NIR transmittance could be dramatically decreased from 40% to 5% (380 nm), from 70% to 5% and from 70% to 10%, respectively, indicating highly efficient and sensitive management. In particular, the application in greenhouse exhibits excellent properties in plants protection, IR cooling and privacy preserving. We believe that this work will pave a facile and low-cost approach for a novel class of integrated smart windows via broadband light modulation.

1. Introduction

Smart windows that can tailor sunlight irradiation have attracted extensive attention not only in academic research but also industrial fields. The most abundant energy sources, i.e. sunlight consists of 5% ultraviolet light (UV), 52% visible light and 43% infrared light (IR). Generally, excessive exposure to UV/IR lights induces the degradation of organic materials, loss of mechanical strength even diseases of human or other creatures [1,2], while selective control of visible light is a necessary choice to achieve energy saving, privacy protection and further space segmentation. Thus smart windows are particularly intriguing as a potential alternative to address these problems. Potential applications include architectural or vehicle windows, house roofs, greenhouse, skylight, etc. Therefore, smart optical materials which are capable of blocking UV and IR lights and manipulating visible light on demand are promising.

Extensive efforts have been devoted for the modulation of lights in specific narrow band. In UV band, the most common approach is the embedding of inorganic UV absorbents (e.g. ZnO [3,4], TiO_2 [5]) in a polymeric matrix [6]. The color/transparency modulation has been extensively studied, involving photonic crystals [7,8] or liquid crystals [9,10] through electric field, oxidation-reduction reactions of chromogenic materials [11,12], phase change materials under heat/light activation [13,14]. In contrast, mechano-driven smart materials exhibit low cost, high efficiency and chemical stability, including surface nanopatterned elastomers [15–19], nano voids inside of elastomer [20–22], cracks on the surface of elastomer [23,24], vertical arranged nanoparticles in elastomers [25,26], IR cooling materials exhibit high solar reflection and high thermal emission, including hierarchical porous polymeric coating [27], phase-change photonic nanostructure [28,29] and phonon resonance effect [30], etc. Moreover, IR transmittance could be effectively blocked via coating of silver nanowires [31], ITO [32] on the surface or inside of PLA, PVB as a result of high IR reflectance. However, these candidates can modulate light only in a specific narrow band, which severely limit the practical applications.

Recently, materials with light-to-heat conversion effects and

* Corresponding author.
E-mail address: liliyang@dhu.edu.cn (L. Yang).

https://doi.org/10.1016/j.solmat.2022.111611
Received 24 September 2021; Received in revised form 6 December 2021; Accepted 14 January 2022
0927-0248/© 2022 Published by Elsevier B.V.

thermochromic effects [33,34] have been studied, but their light transmittance control range is limited (~50%), and the precise control is difficult to achieve. And the surface notch treated elastomer with phase-change VO_2 nanoparticles shows ~40% increase in UV–Vis–NIR transmittance when the strain is up to 100% [35]. Smart film that realize sunlight reflection or heating by adjusting the opening and closing of the nanopores in the black elastomer under the pull/scratch state can achieve effective temperature control, but it is difficult to apply to smart windows due to the inability of displaying transparency [36]. A smart hydroglass that enables to manage the light wavelength over three orders of magnitude, and reversibly switches transmittance in the visible region is reported, while the humid storage environment puts forward higher requirements for its practical application [37]. Therefore, it will be highly desired to design smart membranes with the ability to adjust the light transmittance of UV–Vis–NIR via facile, low-cost approaches.

Previously, we reported a robust smart membrane that could be reversibly switched from highly transparent to opaque under stretching due to the diffused light scattering from micro-/nano voids [20]. Here, an integrated smart membrane with capability of managing the transmittance of UV–Vis–NIR region is reported. As illustrated in Fig. 1A, this smart membrane can be applied as the smart windows of greenhouse, building, skylight etc. for energy saving, privacy protection, plants preserving. The smart membrane consists of upper ITO rich layer for NIR reflection, bottom TiO_2/SiO_2 NPs layer, which embedded in bulk elastomeric PDMS. Rising from the UV absorbing, NIR reflection and Rayleigh scattering, the smart membrane shows moderate UV and IR transmittance and high Vis transmittance under relaxed state, and excellent UV–Vis–NIR modulation under stretching.

2. Experiments

2.1. Materials

Tetraethyl orthosilicate (TEOS, 98%), isopropanol (IPA, 99.8%), ammonium hydroxide (28–30%), ethanol (99%), were purchased from Sinopharm Chemical Reagent Co., Ltd (China). PDMS (Sylgard-184, Dow Corning, USA), ITO nanoparticles (10 nm, Macklin, China), TiO_2 nanoparticles (20 ± 10 nm, Macklin, China) and Rhodamine B (99%, Rhawn, China) were used as received.

2.2. Preparations of smart membranes

Silica NPs were firstly synthesized by the Stöber method. Then a mixed solution in IPA was obtained with SiO_2 and TiO_2 NPs concentrations of 10 mg mL^{-1} and 1 mg mL^{-1}, respectively. Then, the mixed solution was sprayed 20 times by industrial spray gun on the polystyrene (PS) Petri dish at a spray distance of 5 cm and a moving speed of ~5 cm s^{-1}. After that, ITO NPs were dispersed into IPA with a concentration of 10 mg/ml for the 2nd spray coating for 30 times. Dow Corning Sylgard 184 and its curing agent were mixed at a weight ratio 10:1. After degassing, PDMS precursor was cast on the sprayed Petri dish and then cured at 65 °C for 4 h. Finally, the hybrid membrane was carefully peeled from the Petri dish.

2.3. UV-shielding measurement of smart membrane

The degradation behavior of RhB solution in the presence of photocatalyst (TiO_2) under high-pressure mercury lamp (150 W) was conducted to evaluate the UV-shielding performance of membrane. Briefly, 30 mg of TiO_2 and 50 mL of RhB solution (1×10^{-5} M) were mixed for complete dispersion. Smart membrane under different strains was used

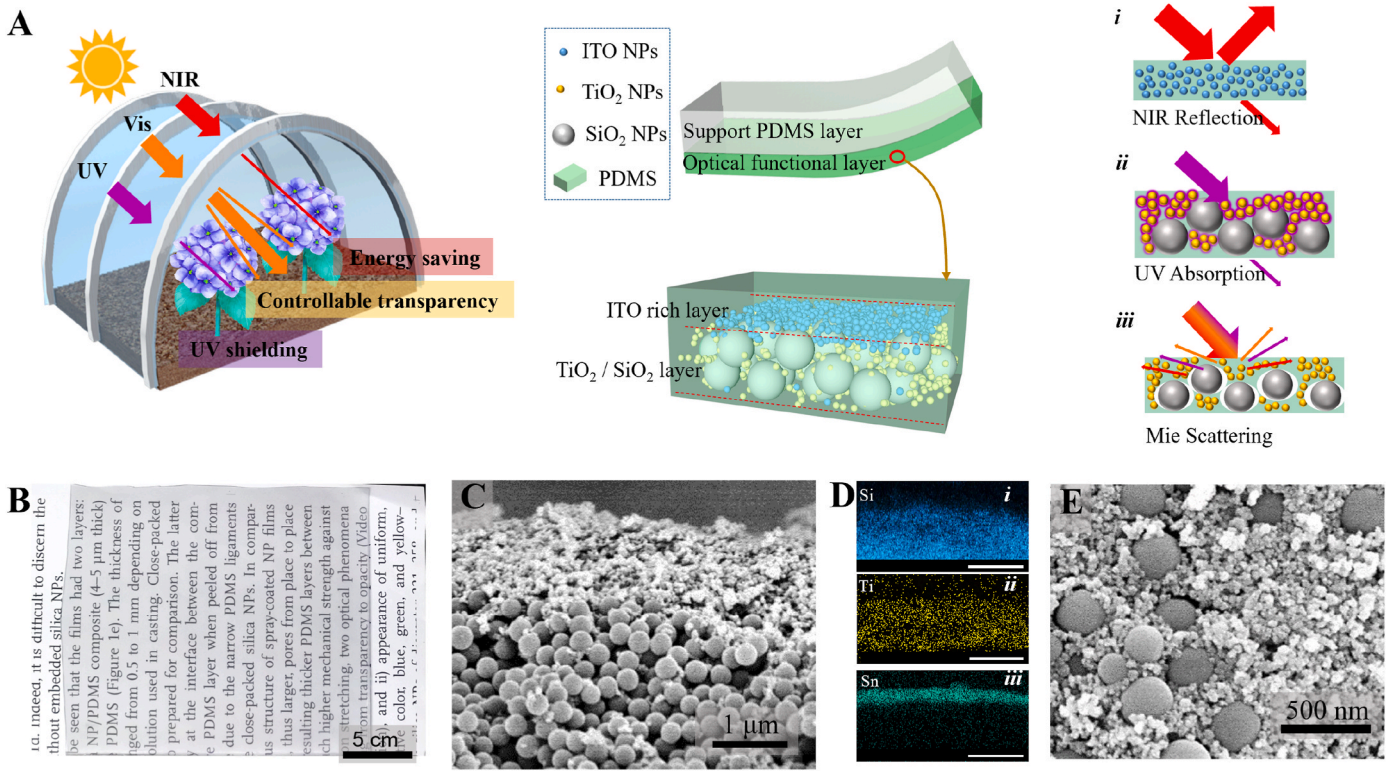

Fig. 1. (A) Schematic of our multifunctional smart membrane as smart window, its composition, and light management mechanism. (*i*) NIR reflection of ITO rich layer, (*ii*) UV absorption of TiO_2 NPs, and (*iii*) light scattering after stretching. (B) Optical image of large-size smart membrane. (C) Cross-sectional SEM image of functional layer in smart membrane. (D) EDS elemental mapping of Si (*i*), Ti (*ii*), Sn (*iii*), scale bar: 2 μm. (E) Surface SEM image of functional layer in smart membrane.

to encloses the entire sample bottle before UV irradiation. The wavelength of UV light was 365 nm, and the light power reaching the surface of the film was 2.26 W/m^2. At given intervals (t), the absorbance of RhB solution at 552 nm was measured by the USB2000 fiber optical spectrometer (Ocean Optics, USA). The UV-shielding performance was calculated as $I=A_t/A_0 \times 100\%$, where A_0 is the initial absorbance of RhB solution and A_t is the absorbance of the remaining RhB solution.

2.4. NIR-shielding measurement of smart membrane

The measurement device was built by a wooden house. The specific test process was to cover the window with a smart membrane under a specific strain. A 50 W halogen tungsten lamp simulated sunlight at a distance of about 50 mm from the top of the film, and records the temperature in the thermal insulation box at a specific time interval.

2.5. Characterization

The surface morphologies and EDS mapping were examined using a field-emission scanning electron microscope (MAIA3, TESCAN, Czech). The surface morphologies of the nanoparticles (TiO_2 and ITO) were examined using a transmission electron microscope (JEM-2100, Japan). The scattering spectra at various strains, the cycle-dependent transmittance and the UV absorbance spectra were collected from a USB2000 fiber optical spectrometer (Ocean Optics, USA) combined with a custom-built stretcher. The UV–Vis–NIR spectra were collected from a UV-3600 spectrometer (Shimadzu, Japan). The haze was collected with an integrating sphere ((INT-36T-2, Changhui Electronic Technology, China). Digital photos were collected using a digital camera (Nikon 1 J5, Japan). The XRD patterns were characterized by X-ray diffractometer (Bruker D8, Germany).

3. Results and discussions

3.1. Design and fabrications of multifunctional smart membrane

As illustrated in Fig. S1, the preparation of multifunctional smart membrane includes three facile steps: spraying of mixed solution involving SiO_2 & TiO_2 NPs, spraying of ITO NPs solution, final casting and curing of PDMS precursor. Therefore, two layers, *i.e.* functional layer and supported PDMS layer, are exhibited (Fig. 1A). The facile industrial-grade process is notably beneficial for the scalable fabrication of smart membrane. Fig. 1B shows a transparent smart membrane with 20 cm × 20 cm × 0.1 cm. The XRD patterns of NPs (Fig. S2) exhibits the amorphous structure of SiO_2 and crystalline structure of ITO and TiO_2. TEM images of TiO_2 and ITO NPs were shown in Fig. S3, indicating the sizes of about 30 nm and 10 nm, respectively. After the first spraying, SiO_2 NPs (~ 290 nm) are arranged with a quasi-ordered structure, while smaller TiO_2 NPs are existing in the voids of silica in the form of small clusters (Fig. 1C and Fig. S4). After the second spraying process, an ITO rich layer is covered on the surface of TiO_2/SiO_2 layers (see Fig. 1C and D), and some areas are even completely covered (Fig. 1E). Importantly, the content of light shielding NPs (TiO_2 and ITO) are small (See Fig. 1C), which can effectively reduce the decrease of transmittance in the visible region.

3.2. Tunable optical property in visible region

Occupying the 52% sunlight radiation, the light management in visible band is so important for the energy saving and privacy protection. In order to clarify the effect of different NPs on the Vis transmittance on relaxed state, Fig. 2A shows the Vis spectra of membranes embedded with various NPs. Due to the very close refractive index of SiO_2 (n = 1.46) and PDMS (1.43), the membrane shows very high transparency (up to 92%). While the transmittance is decreased due to the addition of TiO_2 (n = 2.87) or ITO (n = 1.86) NPs, which is attributed to the enhanced Mie scattering from NPs. However, the smart membrane

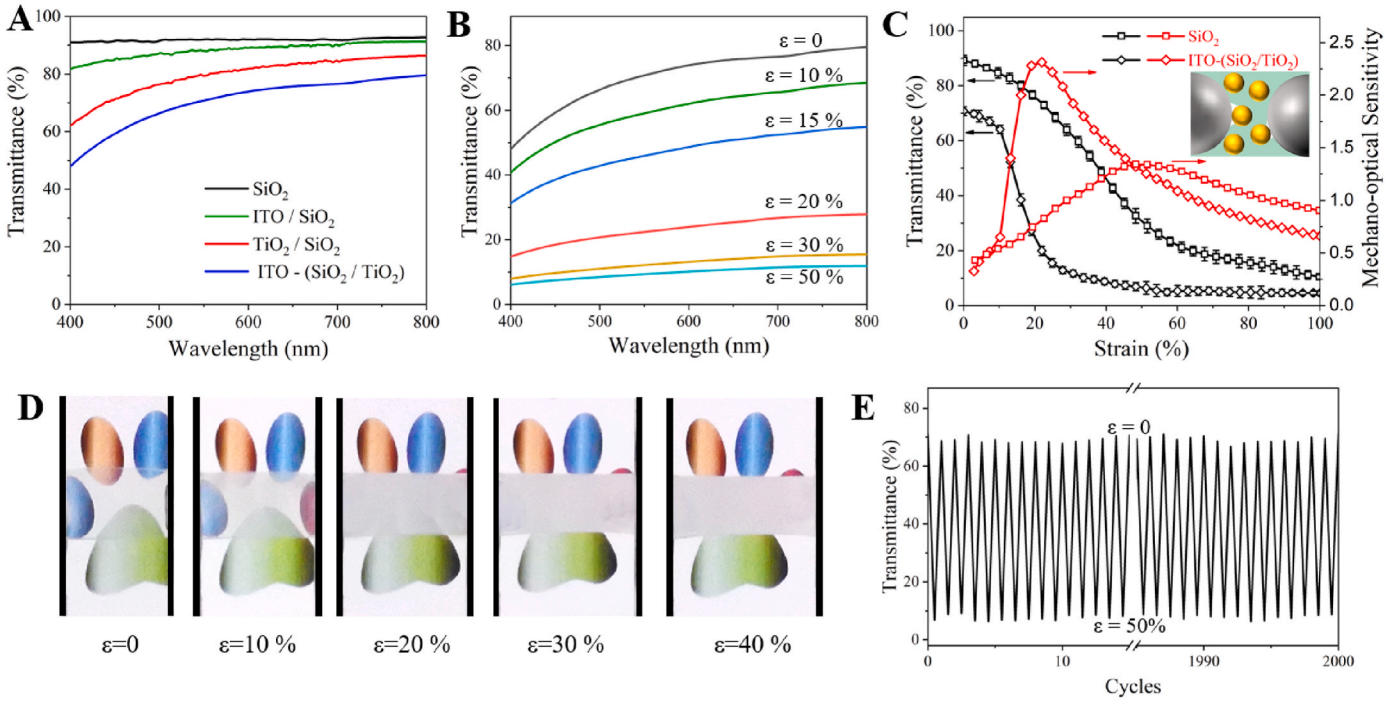

Fig. 2. Visible management ability of smart membrane. (A) Vis Transmittance comparison of various membranes with different NPs. (B)Vis transmittance spectra of smart membrane upon stretching. (C) Transmittance at wavelength of 550 nm and mechano-optical sensitivity of smart membrane comparing with previous smart membrane as a function of applied strain. (D) Optical images of smart membrane at various applied strains. (E) Transmittance at 550 nm versus stretching/release cycle numbers.

involving three kinds of NPs still shows a high transmittance (≥70% at 550 nm) due to the small amount of TiO_2 and ITO NPs. Seen from Video S1, the smart membrane shows a reversible transition between transparent and opaque states under stretching and releasing. Furthermore, the Vis transmittance changes of smart membrane upon stretching is also studied (Fig. 2B). Under the stretching of NPs/PDMS membrane, crescent shaped vacuum cavity ($n = 1$) is formed between NPs and the matrix. In order to understand the Mie scattering resulting from crescent cavity under stretching better, the hazing transmittance is tested and shown in Fig. S6. The increasing haze improves the enhanced Mie scattering under stretching. Based on the spherical and ellipsoid model, the approximate calculations of scattering (details in supporting information) demonstrate that the scattering intensity increases with the volume of cavity under stretching.

Supplementary data related to this article can be found at https://doi.org/10.1016/j.solmat.2022.111611.

Fig. 2C summarized the transmittance decreases at 550 nm and the corresponding mechano-optical sensitivity. The mechano-optical sensitivity (S) can be calculated as follows:

$$S = \left|\frac{T_\varepsilon - T_0}{\varepsilon}\right| \quad (1)$$

where ε is the strain, T_0 and T_ε are the transmittance (wavelength of 550 nm) at initial state ($\varepsilon = 0$) and stretching at a certain strain (ε), respectively. The properties of soft membrane (SiO_2/PMDS) reported in our previous work are also illustrated for comparison. Based on our previous research, the optical tuning is attributed to the Mie scattering from internal cavitation between PDMS and NPs under stretching. It is indicated that a high total transmittance tuning range of ~65% is exhibited, which is little lower than that of SiO_2/PMDS membrane (75%) due to the little loss of original transmittance. However, the transmittance of this smart membrane can be dramatically reduced by ~30% and ~63% at small strain 15% and 40%, respectively. While the SiO_2/PDMS membrane only shows transmittance loss of ~8% and 40% at 15% and 40% strain, respectively. Here we believe that the internal cavitation between PDMS and NPs is easier to form due to the stress concentration because of the incomplete filling of PDMS due to the smaller NPs. Therefore, the mechano-optical sensitivity is enhanced especially in the small strain, which is very important for the applications in smart windows. Fig. 2D also showed the rapid decrease of transmittance of the membrane which transferred to completely opaque at 20% strain during the stretching process. The normal transmittance at 550 nm versus release/stretching cycles was exhibited in Fig. 2E which showed negligible difference of transmittance even after 2000 cycles. This result indicated the excellent robustness of our optical tunable membranes.

3.3. Tunable optical property in UV and NIR region

The UV blocking ability of smart membrane is further explored. In order to clarify the effect of different NPs on the UV transmittance on relaxed state, Fig. 3A shows the UV curves of various membranes. With the adding of TiO_2 and ITO NPs, the UV transmittance of membrane decreased substantially in total three stages (Fig. 3A). Seen from the UV absorbance of TiO_2 and ITO NPs (Fig. S8), a very high UV absorbance of TiO_2 NPs is exhibited and moderate absorbance of ITO is also present. Thus TiO_2 NPs are good at UV blocking, leading to the almost complete blocking of UVC (200–280 nm) and UVB (280–320 nm) and extremely lower transmittance of UVA (320–400 nm). The transmittance spectrum at UV region of the smart membrane during the stretching process is shown in Fig. 3B. It is demonstrated that the UV transmittance of the smart membrane is furtherly decreased with the stretching (0–50%). The UV transmittance at 350 nm is decreased from 30% to 8% and at strain of 20% and 50%. The modulation ability in UVA is greater than

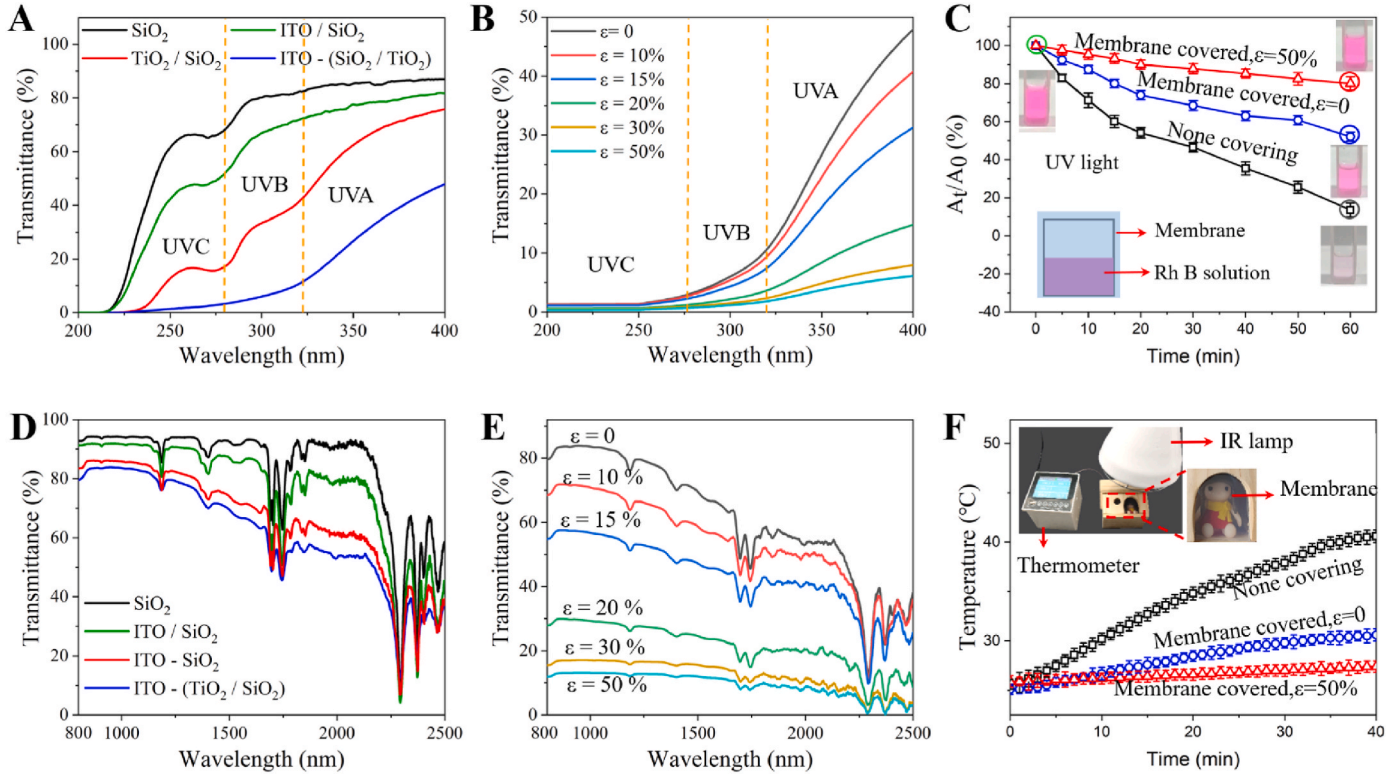

Fig. 3. (A) UV transmittance spectra of various membranes with different NPs. (B) UV transmittance spectra of smart membrane upon stretching. (C) Photodegradation curves of Rh B solutions protected by smart membrane under applied strain. Inset: Schematic diagram of test process and optical images of Rh B under various states. (D) NIR transmittance spectra of various membranes with different NPs. (E) NIR transmittance spectra of smart membrane upon stretching. (F) Temperature change inside the wooden house without or with smart membrane. Inset: optical images of test device.

that in UVC. We believe that this is also mainly due to the Mie scattering from the smaller crescent cavity during the stretching process. The scattering is enhanced with the stretching of smart membrane, leading to the continuous decrease of UV transmittance.

To further investigate the UV-blocking ability of smart membrane, the UV degradation effect of organic dyes is also used to characterize the UV barrier effect of smart membrane. Under the protection of stretched/released smart membrane, the Rhodamine B (Rh B) solution in the presence of photocatalyst is irradiated under a UV lamp, the photocatalytic degradation efficiency is collected (Fig. 3C). As shown in Fig. 3C, with the prolongation of UV irradiation time, the absorption intensity of Rh B solution at 552 nm continues to weaken. After 60 min of UV irradiation, the Rh B solution none covering was almost completely degraded. Under the protection of the relaxed membrane, the degradation rate of Rh B was obviously decreased that shows a drop of 42%, while the Rh B solution protected by the smart membrane in a stretched state shows only 13% degradation. Compared with the original Rh B, the uncovered solution exposed to UV light shows an obvious discoloration due to the large photodegradation, and the RhB protected by released smart membrane displays a relatively little change, while protected by smart membrane under stretched state, the color is very similar to the original solution. This proves the great UV blocking ability in the stretched state.

Besides, the optical management in NIR region is also studied. As illustrated in Fig. 3D, SiO_2/PDMS membrane shows very high transmittance in 800–2200 nm. In order to effectively shield NIR radiation, ITO NPs which exhibit high NIR reflection are added. The membranes with a single layer of ITO and uniform distribution of ITO are both fabricated to investigate the effect of NPs arrangement on the optical properties. Comparing the NIR transmittance of membrane, PDMS itself had absorption in the NIR band of 1500–2500 nm (see Fig. 3D), which is due to molecular vibration. Compared with ITO dispersedly arranged in the gap of SiO_2 particles (ITO/SiO_2), forming an ITO rich layer above the SiO_2 layer (ITO-SiO_2) was an effective means to further reduce the infrared transmittance (Fig. 3D), which was due to the densely arranged ITO layer could better reflect the NIR rays reaching above it and reduce the transmission (see schematic in Fig. 1A). As shown in Fig. 3E, during the stretching process, the NIR transmittance of the smart membrane continues to decrease, which was similar to the UV and visible spectra. We believe that the decrease of NIR transmittance is attributed to the Mie scattering from cavity around NP clusters. It can be seen that the smart membrane shows excellent NIR blocking ability (average NIR transmittance <30%) under small strain (~20%). Furthermore, the NIR shielding ability of smart membrane is explored by recording the temperature of a wooden house with smart window (see Fig. 4D). The thermocouple at the bottom of the wooden house is connected with a thermometer, and the temperature curve inside the wooden house under different state windows was recorded in real time (illustration of Fig. 3F

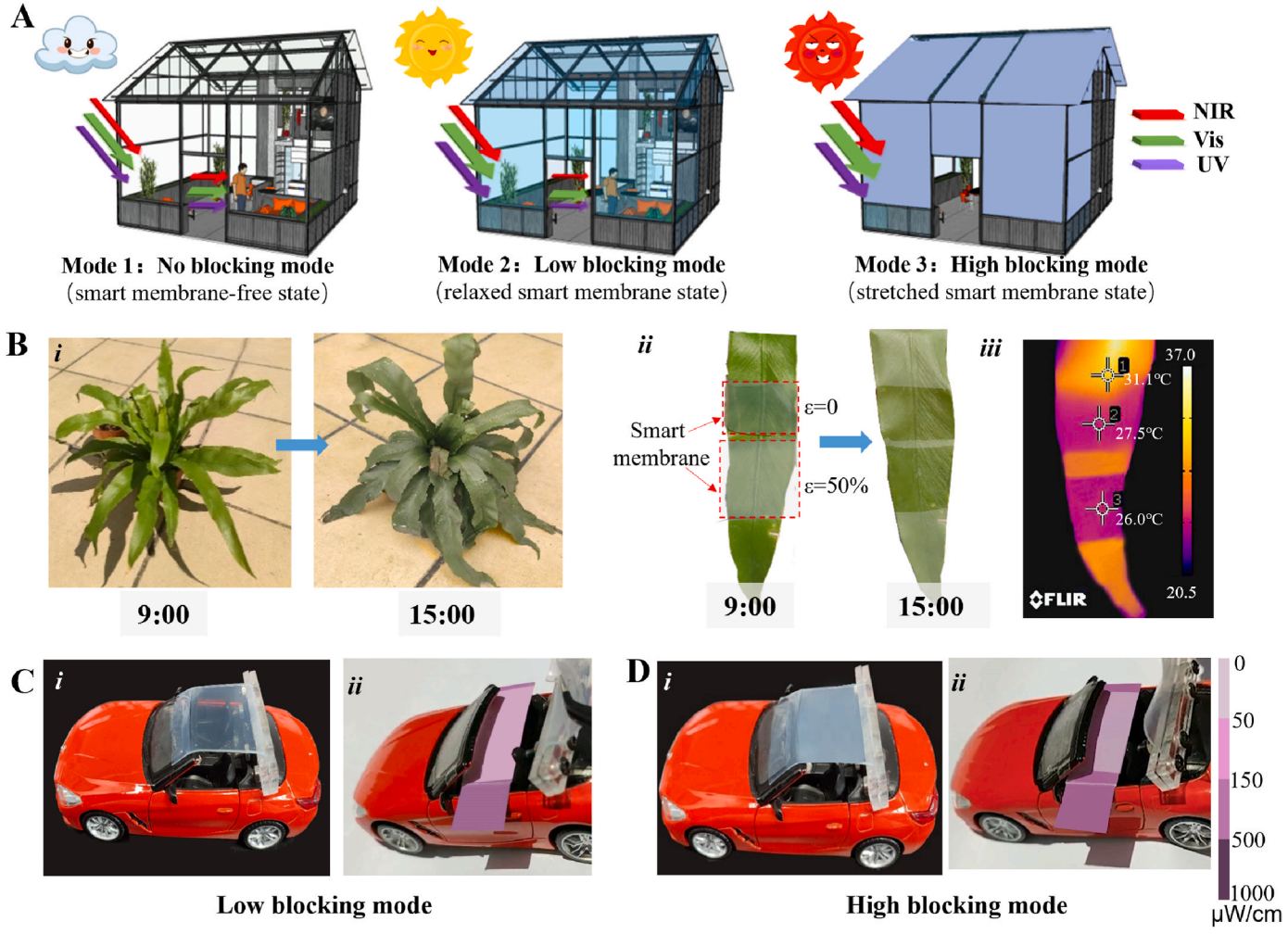

Fig. 4. Schematic and images for potential applications of smart membrane. (A) Schematic illustrations of future application of smart membrane as smart window of sun room. (B) Optical images of (*i*) original Asplenium nidus after sunshine exposure, (*ii*) single leaf covered by smart membrane after same sunshine exposure, and (*iii*) the IR thermal photograph of plant leaf surface protected by smart membrane. (C–D) Optical images of information display (*i*) and UV-shielding effect (*ii*) for applications in automobile skylight under low light blocking mode and high light blocking mode (D).

for the test device). When the initial temperature is close (about 25 °C), the temperature in the cavity none covering increased by 15 °C after the NIR light irradiating for 40 min. In contrast, the temperature rise rate of the wooden house with the unstretched smart membrane as the window significantly drop, the temperature only increased by 5 °C in the same time. However, when the smart film was in an opaque state with 50% strain, the temperature only increased by 1 °C. Such significant cooling effect is ascribed to the reason that the smart membrane simultaneously isolates visible and NIR light and decreases the solar energy absorbed by the inner thermometer.

In order to study the stability at UV and NIR band, the UV–Vis–NIR transmittance of smart membrane before and after 2000 cycles of stretching is shown in Fig. S9. The optical property is almost unchanged, indicating the structural stability during stretching. Moreover, the optical properties of membrane before and after outdoor illumination for 20 days is compared in Fig. S10. The retained transmittance also demonstrates a good chemical stability for applications.

3.4. Potential applications as smart windows

Fig. 4A illustrates there are three modes for the applications as smart window to satisfy different requirements under different environments. In cloudy days, the smart membrane is rolled up, showing a fully transparent state and providing sufficient solar radiation (Fig. 4A-*i*). In sunny days, the sun room is covered with the smart membrane at relaxed state (Fig. 4A-*ii*). The low light blocking mode is displayed, in which UV and NIR lights are effectively blocked while visible lights can transmit. Thus the plants health is keeping while energy consumption is moderately reduced. More, in hot days, the high blocking mode is triggered when the smart membrane is stretched. Based on above experimental results, the broadband UV–Vis–NIR radiation could be effectively restrained and the inhibition degree varies with the strain. Under this mode, the smart membrane can achieve UV protection, lowering the indoor temperature and protecting privacy indoor (Fig. 4A-*iii*).

This smart membrane is especially suitable for the smart windows for sun rooms and greenhouses. Seen from Fig. 4B, Asplenium nidus leaves are shriveled due to the exposure of sun shine for 6 h. In order to verify the protection of smart membrane, the relaxed and stretched smart membrane are placed at a distance of 20 mm above the leave surface. After same 6 h of strong sunlight, the green color of the leave covered by the smart membrane is obviously brighter and more vitality than uncovered (Fig. 4B-*iii*). The surface temperature of the leaf after 1h exposure to sunlight was obtained by an infrared camera (Fig. 4B-*ii*). The surface temperature of uncovered leave is as high as 31.1 °C. In contrast, the surface temperature of leave covered with relaxed smart membrane is 27.5 °C, while the surface temperature is only 26.0 °C when the smart film is stretched (50%). It is indicated that the smart membrane can also effectively block NIR light, thereby reducing the temperature and protecting plants.

In addition, the potential application of our smart membrane as smart skylight is also a good choice. As illustrated in Fig. 4C-*i*, when the smart membrane is relaxed, the interior of the car is in a relatively low UV and NIR state, while the details of the car can be seen clearly. As shown in Fig. 4C-*ii*, the UV display card of the sports car seat shows that the UV light intensity of the protected area is significantly lower than the unprotected area. When the smart membrane is stretched, the UV and NIR transmittance in the car is further reduced, and privacy protection is also provided (see Fig. 4D-*i*). As shown in Fig. 4D-*ii*, the UV intensity of the protected area by the stretched smart membrane is significantly lower than that of the unprotected area. The application of smart films to closed environments such as buildings and semi-closed environments can achieve good UV blocking capabilities, and is of great significance for reducing the temperature and providing the required visible blocking capabilities.

4. Conclusions

In summary, we present an integrated smart membrane with UV–Vis–NIR broadband light modulation for multifunctional smart windows. This smart membrane consisting of SiO_2, TiO_2 and ITO NPs in elastomeric PDMS is fabricated via spray coating and casting process. In relaxed state, the smart membrane exhibits moderate UV and NIR transmittance and high Vis transmittance. While under stretched state, due to the Mie scattering from nanocavitation, the UV–Vis–NIR transmittance shows excellent modulation. UV, Vis and NIR transmittance under stretching (50%) could be dramatically decreased from 40% to 5% (380 nm), from 70% to 5% and from 70% to 10%, respectively. Overall, our study provides a low-cost, integrated smart membrane in the potential applications in greenhouse, skylight etc. for energy conservation, privacy protection and organism healthcare.

CRediT authorship contribution statement

Yang Liu: Methodology, Writing – original draft. **Shaoxin Song:** Methodology. **Hyunsik Yoon:** Writing – review & editing. **Mingxia Liu:** Methodology. **Lili Yang:** Conceptualization, Project administration, Writing – review & editing. **Dengteng Ge:** Writing – review & editing, Supervision, Project administration.

Declaration of competing interest

The authors declare that they have no known competing financial interests or personal relationships that could have appeared to influence the work reported in this paper.

Acknowledgements

This work is supported by the National Natural Science Foundation of China 11774049and 51973033, and the Fundamental Research Funds for the Central Universities 2232021D-02.

Appendix A. Supplementary data

Supplementary data to this article can be found online at https://doi.org/10.1016/j.solmat.2022.111611.

References

[1] M. Zayat, P. Garcia-Parejo, D. Levy, Preventing UV-light damage of light sensitive materials using a highly protective UV-absorbing coating, Chem. Soc. Rev. 36 (2007) 1270–1281, https://doi.org/10.1039/b608888k.
[2] L.R. Sklar, F. Almutawa, H.W. Lim, I. Hamzavi, Effects of ultraviolet radiation, visible light, and infrared radiation on erythema and pigmentation: a review, Photochem. Photobiol. Sci. 12 (2013) 54–64, https://doi.org/10.1039/c2pp25152c.
[3] X.J. Huang, X.F. Zeng, J.X. Wang, J.F. Chen, Transparent dispersions of monodispersed ZnO nanoparticles with ultrahigh content and stability for polymer nanocomposite film with excellent optical properties, Ind. Eng. Chem. Res. 57 (2018) 4253–4260, https://doi.org/10.1021/acs.iecr.7b04878.
[4] E. Olson, Y. Li, F.Y. Lin, A. Miller, F. Liu, A. Tsyrenova, D. Palm, G.W. Curtzwiler, K.L. Vorst, E. Cochran, S. Jiang, Thin biobased transparent UV-blocking coating enabled by nanoparticle self-assembly, ACS Appl. Mater. Interfaces 11 (2019) 24552–24559, https://doi.org/10.1021/acsami.9b05383.
[5] J.W. Choi, J.H. Lee, Selectively UV-blocking and visibly transparent adhesive films embedded with TiO2/PMMA hybrid nanoparticles for displays, Materials 13 (2020) 5273, https://doi.org/10.3390/ma13225273.
[6] D. Chen, W. Sun, C. Qian, A.P.Y. Wong, L.M. Reyes, G.A. Ozin, UV-blocking photoluminescent silicon nanocrystal/polydimethylsiloxane composites, Adv. Opt. Mater. 5 (2017), 1700237, https://doi.org/10.1002/adom.201700237.
[7] M.E. McConney, V.P. Tondiglia, L.V. Natarajan, K.M. Lee, T.J. White, T.J. Bunning, Electrically induced color changes in polymer-stabilized cholesteric liquid crystals, Adv. Opt. Mater. 1 (2013) 417–421, https://doi.org/10.1002/adom.201300111.
[8] Q. Fu, H. Zhu, J. Ge, Electrically tunable liquid photonic crystals with large dielectric contrast and highly saturated structural colors, Adv. Funct. Mater. 28 (2018), 1804628, https://doi.org/10.1002/adfm.201804628.
[9] C.H. Yang, S. Zhou, S. Shian, D.R. Clarke, Z. Suo, Organic liquid-crystal devices based on ionic conductors, Mater. Horiz 4 (2017) 1102–1109, https://doi.org/10.1039/c7mh00345e.

[10] S.M. Guo, X. Liang, C.H. Zhang, M. Chen, C. Shen, L.Y. Zhang, X. Yuan, B.F. He, H. Yang, Preparation of a thermally light-transmittance-controllable film from a coexistent system of polymer-dispersed and polymer-stabilized liquid crystals, ACS Appl. Mater. Interfaces 9 (2017) 2942–2947, https://doi.org/10.1039/c7mh00345e.

[11] A.T. Smith, H. Ding, A. Gorski, M. Zhang, P.A. Gitman, C. Park, Z. Hao, Y. Jiang, B. L. Williams, S. Zeng, A. Kokkula, Q. Yu, G. Ding, H. Zeng, L. Sun, Multi-color reversible photochromisms via tunable light-dependent responses, Matter 2 (2020) 680–696, https://doi.org/10.1016/j.matt.2019.12.006.

[12] M.J. Kang, E.G. Santoro, Y.S. Kang, Enhanced efficiency of functional smart window with solar wavelength conversion phosphor-photochromic hybrid film, ACS Omega 3 (2018) 9505–9512, https://doi.org/10.1021/acsomega.8b01091.

[13] L.Y.L. Wu, Q. Zhao, H. Huang, R.J. Lim, Sol-gel based photochromic coating for solar responsive smart window, Surf. Coat. Technol. 320 (2017) 601–607, https://doi.org/10.1016/j.surfcoat.2016.10.074.

[14] H.N. Apostoleris, M. Chiesa, M. Stefancich, Improved transparency switching in paraffin–PDMS composites, J. Mater. Chem. C 3 (2015) 1371–1377, https://doi.org/10.1016/j.surfcoat.2016.10.074.

[15] E. Lee, M. Zhang, Y. Cho, Y. Cui, J. Van der Spiegel, N. Engheta, S. Yang, Tilted pillars on wrinkled elastomers as a reversibly tunable optical window, Adv. Mater. 26 (2014) 4127–4133, https://doi.org/10.1002/adma.201400711.

[16] S.G. Lee, D.Y. Lee, H.S. Lim, D.H. Lee, S. Lee, K. Cho, Switchable transparency and wetting of elastomeric smart windows, Adv. Mater. 22 (2010) 5013–5017, https://doi.org/10.1002/adma.201002320.

[17] G. Lin, P. Chandrasekaran, C. Lv, Q. Zhang, Y. Tang, L. Han, J. Yin, Self-similar hierarchical wrinkles as a potential multifunctional smart window with simultaneously tunable transparency, structural color, and droplet transport, ACS Appl. Mater. Interfaces 9 (2017) 26510–26517, https://doi.org/10.1021/acsami.7b05056.

[18] H. Xu, C. Yu, S. Wang, V. Malyarchuk, T. Xie, J.A. Rogers, Deformable, programmable, and shape-memorizing micro-optics, Adv. Funct. Mater. 23 (2013) 3299–3306, https://doi.org/10.1002/adfm.201203396.

[19] J. Li, J. Shim, J. Deng, J.T.B. Overvelde, X. Zhu, K. Bertoldi, S. Yang, Switching periodic membranes via pattern transformation and shape memory effect, Soft Matter 8 (2012) 10322–10328, https://doi.org/10.1039/c2sm25816a.

[20] D.T. Ge, E. Lee, L.L. Yang, Y. Cho, M. Li, D.S. Gianola, S. Yang, A robust smart window: reversibly switching from high transparency to angle-independent structural color display, Adv. Mater. 27 (2015) 2489–2495, https://doi.org/10.1002/adma.201500281.

[21] H.N. Kim, D. Ge, E. Lee, S. Yang, Multistate and on-demand smart windows, Adv. Mater. 30 (2018), 1803847, https://doi.org/10.1002/adma.201803847.

[22] Y. Jiang, S. Zeng, Y. Yao, S. Xu, Q. Dong, P. Chen, Z. Wang, M. Zhang, M. Zhu, G. Xu, H. Zeng, L. Sun, Dynamic optics with transparency and color changes under ambient conditions, Polymers 11 (2019) 103, https://doi.org/10.3390/polym11010103.

[23] S. Zeng, D. Zhang, W. Huang, Z. Wang, S.G. Freire, X. Yu, A.T. Smith, E.Y. Huang, H. Nguon, L. Sun, Bio-inspired sensitive and reversible mechanochromisms via strain-dependent cracks and folds, Nat. Commun. 7 (2016) 11802, https://doi.org/10.1038/ncomms11802.

[24] Z. Mao, S. Zeng, K. Shen, A.P. Chooi, A.T. Smith, M.D. Jones, Y. Zhou, X. Liu, L. Sun, Dynamic mechanochromic optics with tunable strain sensitivity for strain-responsive digit display, Adv. Opt. Mater. 8 (2020), 2001472, https://doi.org/10.1002/adom.202001472.

[25] A.C.C. Rotzetter, R. Fuhrer, R.N. Grass, C.M. Schumacher, P.R. Stoessel, W.J. Stark, Micro mirror polymer composite offers mechanically switchable light transmittance, Adv. Eng. Mater. 16 (2014) 878–883, https://doi.org/10.1002/adem.201300478.

[26] J. Li, X. Lu, Y. Zhang, X. Ke, X. Wen, F. Cheng, C. Wei, Y. Li, K. Yao, S. Yang, Highly sensitive mechanoresponsive smart windows driven by shear strain, Adv. Funct. Mater. 31 (2021), 2102350, https://doi.org/10.1002/adem.201300478.

[27] X. Huang, N. Li, J. Wang, D. Liu, J. Xu, Z. Zhang, M. Zhong, Single nanoporous $MgHPO_4.1.2H_2O$ for daytime radiative cooling, ACS Appl. Mater. Interfaces 12 (2020) 2252–2258, https://doi.org/10.1021/acsami.9b14615.

[28] S. Chandra, D. Franklin, J. Cozart, A. Safaei, D. Chanda, Adaptive multispectral infrared camouflage, ACS Photonics 5 (2018) 4513–4519, https://doi.org/10.1021/acsphotonics.8b00972.

[29] A. Tittl, A.K. Michel, M. Schaferling, X. Yin, B. Gholipour, L. Cui, M. Wuttig, T. Taubner, F. Neubrech, H. Giessen, A switchable mid-infrared plasmonic perfect absorber with multispectral thermal imaging capability, Adv. Mater. 27 (2015) 4597–4603, https://doi.org/10.1002/adma.201502023.

[30] Y. Zhai, Y.G. Ma, S.N. David, D.L. Zhao, R.N. Lou, G. Tan, R.G. Yang, X.B. Yin, Scalable-manufactured randomized glass-polymer hybrid metamaterial for daytime radiative cooling, Science 355 (2018) 1062–1066, https://doi.org/10.1126/science.aai7899.

[31] S. Lin, H. Wang, X. Zhang, D. Wang, D. Zu, J. Song, Z. Liu, Y. Huang, K. Huang, N. Tao, Z. Li, X. Bai, B. Li, M. Lei, Z. Yu, H. Wu, Direct spray-coating of highly robust and transparent Ag nanowires for energy saving windows, Nano Energy 62 (2019) 111–116, https://doi.org/10.1016/j.nanoen.2019.04.071.

[32] A. Llordes, G. Garcia, J. Gazquez, D.J. Milliron, Tunable near-infrared and visible-light transmittance in nanocrystal-in-glass composites, Nature 500 (2013) 323–326, https://doi.org/10.1038/nature12398.

[33] H. Zhu, L. Wang, Smart window based on Cu7S4/hydrogel composites with fast photothermal response, Sol. Energy Mater. Sol. Cells 202 (2019), 110109, https://doi.org/10.1016/j.solmat.2019.110109.

[34] D. Cao, C. Xu, W. Lu, C. Qin, S. Cheng, Sunlight-driven photo-thermochromic smart windows, Sol. RRL 2 (2018), 1700219, https://doi.org/10.1002/solr.201700219.

[35] Y. Ke, Y. Yin, Q. Zhang, Y. Tan, P. Hu, S. Wang, Y. Tang, Y. Zhou, X. Wen, S. Wu, T. J. White, J. Yin, J. Peng, Q. Xiong, D. Zhao, Y. Long, Adaptive thermochromic windows from active plasmonic elastomers, Joule 3 (2019) 858–871, https://doi.org/10.1016/j.joule.2018.12.024.

[36] H. Zhao, Q. Sun, J. Zhou, X. Deng, J. Cui, Switchable cavitation in silicone coatings for energy-saving cooling and heating, Adv. Mater. 32 (2020), 2000870, https://doi.org/10.1002/adma.202000870.

[37] Z. Lei, B. Wu, P. Wu, Hierarchical network-augmented hydroglasses for broadband light management, Research 2021 (2021) 1–12, https://doi.org/10.34133/2021/4515164.